Abstract

Introduction: Earlier evaluation of treatment response to radiation therapy (RT) could lead to better prognoses for cancer patients. Tumors exhibit vascular remodeling while they are growing, which indicates an increase in the expression of angiogeneic proteins such as vascular endothelial growth factor (VEGF). We hypothesize that molecular imaging using contrast enhanced ultrasound (CEUS) is able to detect longitudinal changes in tumor microvasculature after radiation therapy before changes in tumor volume or vascular density actually manifest.

Methods: Fibrosarcoma tumors were implanted in Female Fischer 344 rats (n=10). When the tumors reached approximately 1 cm in diameter, they were either treated with 20 Gy broad beam radiation (n=8) or left untreated (control, n=2). All animals were imaged prior to, and serially twice a week after, treatment. Imaging consisted of VEGFR-2 molecular imaging with contrast enhanced ultrasound. The molecular targeting for each timepoint was quantified.

Results: Molecular targeting assessment showed no significant increase in VEGFR-2 expression before tumor regrowth. Moreover, molecular targeting, peak perfusion, and area under the time-intensity curve (TIC) decreased throughout the duration of the study.

Discussion/Conclusion: The ability of molecular imaging to detect changes in tumor microvasculature was not verified in this study. However, it is not possible to conclude a true negative finding among the results due to several confounding variables and study limitations, such as unpredictable tumor response, microbubble inconsistences, and varying perfusion rates. The results from this study indicate that it needs to be modified and repeated. Therefore, although VEGFR-2 has the potential to be a biomarker for tumor response to radiation therapy, it is not possible to definitively determine its utility as a means of tumor microvasculature assessment from this study alone.

1. Introduction

One of the biggest initiatives in modern day healthcare is precision medicine [1]. Consider two patients who receive identical treatment for the same type of cancer. Patient A responds to therapy and enters remission, while Patient B develops resistance to treatment. Precision medicine is based on the idea that patients respond to treatment differently due to individual variances in environment, genetics, and lifestyle [1]. If the two patients were being treated according to precision medicine, they would have received individually tailored treatment based on genetic testing and bioinformatics [1]. Another way to apply precision medicine is to assess an individual's initial response and then tailor subsequent treatment based on previous patients who exhibited similar behavior, ensuring maximum treatment efficacy [2]. Moreover, the ability to promptly identify when a treatment is failing is beneficial as it increases the chances of tailoring the treatment approach [2]. One of the applications of precision medicine is for the treatment of cancer.

Radiation therapy (RT) is one of the most common forms of cancer treatment [3]. RT works by inducing double stranded breaks in the DNA of the treated cells, so they can no longer proliferate. Approximately 50% of all cancer patients receive some type of RT throughout their treatment, with either curative or palliative intent [3]. Due to genetic and environmental factors, each patient will respond to RT uniquely. There are many parameters that need to be considered when determining what type of RT will be most effective for a specific patient [3]. Examples of such parameters include the type and stage of the cancer, location in body, proximity of tumor to sensitive areas and patient's medical history.

Currently, response to RT is assessed using the Response Evaluation Criteria In Solid Tumors (RECIST) guidelines [4]. This involves measuring changes in tumor volume via MRI or CT. Unfortunately, measurable changes in tumor size do not manifest until weeks or months

after treatment. There is a need to determine a faster way to predict response to radiation therapy [5]. This information will allow the clinician to adjust the parameters necessary in order to find the radiotherapy that is best suited for the patient or change treatment modality altogether. Cancer treatment is time sensitive – weeks of ineffective treatment could result in further development and spreading of the cancer, reducing the likelihood for remission [5]. The personalization of radiation therapy treatment is important because it has the potential to assess treatment response earlier and improve prognoses – if a treatment is not working for a patient, it can be modified or changed before the disease advances [6]. This can also be utilized to minimize exposure to ineffective radiation.

There have been studies done to look at other metrics by which we can assess tumor response to radiation therapy besides changes in tumor volume [7]. One of these metrics is microvasculature assessment. After tumors are treated with radiation therapy, they can exhibit a period of vascular remodeling that is marked by angiogenesis [5]. In 2017, Kasoji, et al conducted a preclinical study in which rats were implanted with fibrosarcoma tumors and treated with radiation therapy to determine if changes in vascular density correlated with treatment response [5]. Vascular density was measured at regular intervals after treatment. Animals were grouped as local control (tumor was gone by the end of the study), local failure (tumors shrunk initially but then regrew), or untreated. The results of the study showed that changes in vascular density occurred earlier than changes in tumor volume [5]. The local failure group exhibited an increase in vascular density (at around day 10) before tumor volume regrowth (> day 20) while the local control group did not exhibit such increase. The study demonstrated the potential to predict treatment response to radiation therapy earlier than tumor volume measurements by assessing changes in tumor microvasculature [5].

One proposed pathway by which vascular density increases within tumors is through vascular endothelial growth factor (VEGF) [8]. VEGF is a signaling molecule that mediates angiogenesis. Angiogenesis is the formation of new blood vessels from pre-existing vessels. Solid tumors are dependent on angiogenesis for growth. Angiogenesis can be triggered through inflammation and/or hypoxia [8]. Inflammation plays a role in approximately 15-20% of malignancies. These malignancies are characterized by the rapid recruitment and infiltration of macrophages. The tumor-associated macrophages (TAMs) then activate signaling molecules such as VEGF to stimulate tumor proliferation [8]. Moreover, since tumors are growing rapidly, they often become hypoxic and need new blood vessels rapidly for sufficient oxygen supply. Hypoxic tumors release Hypoxia-Inducible-Factor-1 (HIF-1), which also activates angiogenesis [9]. It has been shown that higher levels of VEGF are associated with increased angiogenesis and cancer proliferation [10]. Activation of VEGF results in the recruitment of pericytes, contractile cells that wrap around the surface of blood vessels. It is known that tumor pericytes contribute to angiogenesis; the exact mechanism by which this occurs is beyond the scope of this paper [11].

We hypothesize that contrast enhanced ultrasound (CEUS) is able to detect longitudinal changes in tumor microvasculature after radiation therapy. The advantages of using ultrasound include that it is inexpensive compared to other imaging modalities, it is portable and thus readily accessible throughout hospitals/other healthcare settings, and it is free of ionizing radiation. Due to tumor heterogeneity, 2D tumor scans can be inaccurate [12]. 3D ultrasound techniques are being developed to image all aspects of a tumor [12]. Moreover, normal b-mode ultrasound is limited by depth penetration and resolution when compared to other imaging modalities such as MRI or CT. Traditional b-mode ultrasound is also unable to differentiate blood from tissue or differentiate between malignant and benign lesions [13]. Conversely,

contrast-enhanced ultrasound (CEUS) can be used to increase the contrast to tissue ratio and thus provide accurate blood flow information [14]. Microbubble contrast agents consist of a phospholipid shell filled with an inert gas and exhibit very high echogenicity compared to soft body tissue and blood. Microbubbles are 1-3 μm in diameter, confining them to the intravascular space, and exhibit a nonlinear super harmonic acoustic response when excited at a high enough energy [14]. The large echogenicity of the microbubbles enhances the reflection of the ultrasound waves, which causes the transducer to receive a larger amplitude signal than if the microbubbles had not been used. This enhances the overall image produced, allowing the user to visualize tissue vasculature with increased sensitivity and specificity [14].

It is possible to attach a biomarker to microbubbles to assess molecular changes, a technique known as molecular imaging [15]. A binding ligand such as an antibody or peptide, is attached to the shell of the microbubble. This allows the microbubble to preferentially bind to the receptors on the vessel endothelium of the tissue of interest. The acoustic backscatter of the bound microbubbles can be quantified and provides a metric with which to quantify expression levels of a specific biomarker of interest [15]. In particular, VEGF is known to bind to its receptor, VEGFR-2 (vascular endothelial growth factor receptor 2) [7]. VEGF is attached to the outside shell of the microbubble so that it can bind to the receptor in vivo to quantify VEGFR-2 expression.

Based on previous preclinical work, tumors begin to show an increase in vascular density around day 10 [5]. These changes in tumor microvasculature that occur before changes in tumor volume indicate that there should also be changes in the angiogenic signaling pathways and VEGFR-2 expression, perhaps even earlier than changes in vascular density. Therefore, we

hypothesize that molecular imaging may be able to predict longitudinal response to radiation therapy before changes in vascular density or tumor volume.

In this study, molecular imaging via contrast enhanced ultrasound (CEUS) is used to assess changes in VEGFR-2 expression. The microbubble contrast agents had VEGF attached to their outer shell such that they bound to VEGFR-2. The animal and tumor model used in this study was the same as in [5]. Animals were imaged serially after treatment to assess changes in molecular targeting.

2. Materials and Methods

A pilot study was conducted prior to the study that is described subsequently. **Supplemental Information S.1 - S.3** describes the parameters of the pilot study and discusses the results.

2.1 Animal and Tumor Models

All animal experimental procedures were approved by the University of North Carolina at Chapel Hill Animal Care and Use Committee. Rat fibrosarcoma tumor tissue provided by the Dewhirst Lab at Duke University was subcutaneously implanted into the right flank of female Fischer 344 rats (n=10) (Charles River Laboratories, Durham, NC) as previously described [16].

2.2 Radiation Therapy Parameters

Once tumors were approximately 1 cm, animals (n=8) were treated with a single dose of 20 Gy broad beam radiation, following a previously published protocol briefly described hereafter [5]. The remaining were left as untreated controls (n=2). The rats were anesthetized using 2% vaporized isoflurane and placed on a heating pad throughout treatment. They were positioned and angled using a rotatable rat positioning table (VisualSonics, Toronto, Canada) such that the tumor was irradiated with minimal exposure to the rest of the animal. The rats were

treated with a Primus II clinical linear accelerator (Siemens Healthcare, Malvern, PA), with a dose prescription of 6 MV photons. The dose rate was 300 mu/min, and the field size was 2x2 cm. The source-to-skin-distance was 100 cm. The animals were monitored daily for the first two weeks post treatment, and then every third day afterwards. The animals were given calorie-rich and hydrating gel in addition to regular protein pellets to prevent excessive weight loss and dehydration caused by the radiation.

2.3 Targeted Microbubble Contrast

Microbubbles were made in house as per [15]. The original formula used to make non-targeted microbubbles involves 90 mole percent 1,2-disteraoyl-sn-glycero-3-phosphocholine (DSPC) (Avanti Polar Lipids, Alabaster, CA) and 10 mole percent 1,2-disteroyl-sn-glycero-3-phospho-ethanolamine-N-[methoxy(polyethylene glycol)-2000] (DSPE-PEG2000) (Avanti Polar Lipids, Alabaster, CA) dissolved in 15% (v/v) propylene glycol, 5% (v/v) glycerol) in phosphate buffered saline (PBS) [15].

A sulfhydryl-activated lipid is necessary to attach the ligand needed to make targeted bubbles [15]. Traut's reagent was used to convert DSPE-PEG2000-Amine to sulfhydryl-activated DSPE-PEG2000-Thiol. The original formula was modified such that the lipid solution now consisted of 90% DSPC, 9.8% DSPE-PEG2000, and 0.2% DSPE-PEG2000-Thiol [15]. The lipid solution was gas exchanged with decafluorobutane (DFB) (Fluoromed, Round Rock, TX) and shaken in glass vials using a VialMix (Bristol-Myers Squibb Medical Imaging, North Billerica, MA). NeutrAvidin (Pierce Biotechnology, Rockford, IL) is a commercially available form of avidin that is more specific than its natural form. A key characteristic of NeutrAvidin is that it contains an available maleimide group that will react with sulfhydryl containing molecules [15]. A molar excess of NeutrAvidin was reacted with the sulfhydryl-activated ultrasound

contrast, which created NeutrAvidin-coated microbubbles. NeutrAvidin-coated microbubbles were then reacted with biotinylated sc-VEGF (single-chain VEGF) (SibTech, Brookfield, CT). The scVEGF is an engineered construct that contains an isoform of VEGF-A, which binds to both VEGFR-1 and VEGFR-2 [17]. It is known that VEGFR-2 is the receptor that appears to mediate almost all cellular response to VEGF [18]. This resulted in a microbubble with VEGF as the targeting ligand so that it bound to VEGFR-2.

Control contrast was also made in house by modifying a previously published protocol [15]. Two separate types of control contrast were made for this study. The procedure to make these bubbles was the same as described above, except instead of attaching biotinylated scVEGF to the NeutrAvidin-coated microbubbles, goat anti-chicken IgY was attached (Thermo Fisher Scientific, Waltham, MA). IgY (Immunoglobulin Y) is a protein found in birds that should not bind to anything in a rat. The other type of control contrast used was NeutrAvidin-coated microbubbles that did not have any biomarker attached to them.

2.4 Pre-dosing

The microbubbles used in this study have an outer shell that consists of polyethylene glycol (PEG) [15]. It has been shown that PEG is detected by the immune system, which causes the accelerated blood clearance (ABC) effect [19]. The ABC effect was observed in the pilot study **(Supplemental Information S.3)**. As a result, the animals in this cohort were pre-dosed with microbubbles in order to minimize ABC, which affects microbubble circulation times. A catheter was placed in the tail-vein of the animals and they were given a bolus injection of 4 x 10^7 microbubbles (not targeted microbubbles: 90% DSPC, 10% DSPE-PEG2000). This was done every day, for four days prior to the first day of imaging.

2. 5 Imaging Parameters

The concentration of the targeted microbubbles was measured before imaging each day using the AccuSizer 780A (Particle Sizing Systems, Santa Barbara, CA). The injected volume of microbubbles was adjusted based on the daily concentration such that each injection contained approximately 4 x 10^7 microbubbles. This value was chosen based on experimental trial and error from the pilot study (**Supplemental Information S.1**), such that sufficient targeting was present. A 15L8 linear array transducer was used with the Acuson Sequoia 512 ultrasound system (Siemens, Mountain View, CA). A motion stage in conjunction with a custom LabVIEW program (National Instruments, Austin, TX) were used to step the transducer through the entire length of the tumor.

2.6 Imaging Timeline

The animals were imaged with VEGF targeted contrast on the morning prior to radiation treatment (baseline day 0) (**Figure 1)**. They were treated with radiation therapy in the evening on that same day, and then imaged the next morning (day 1). Afterwards, animals were imaged two times a week thereafter until the tumors reached 2 cm in diameter (endpoint of the study).

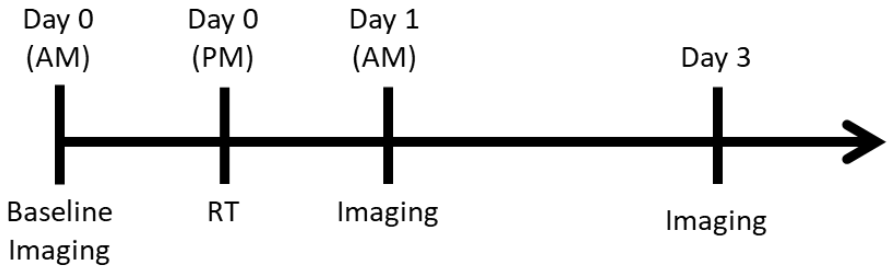

Figure 1*. Imaging timeline. Animals were baseline imaged in the morning prior to treatment (day 0). They were treated with radiation therapy (RT) in the evening on that same day and then imaged the next morning. Subsequent imaging sessions occurred twice a week.*

2.7 Imaging Procedure

Rats were anesthetized with 2% vaporized isoflurane. The rat was then moved to a heating pad. A tail vein catheter was inserted in order to allow for bolus injection of microbubbles. The area surrounding the tumor was shaved and ultrasound gel was placed on the shaved area. The rat was then positioned such that the tumor was in the center of a b-mode image.

Multiple 3D volumetric scans were taken before and after contrast injection. A preliminary b-mode scan was taken before any contrast was injected. Cadence Pulse Sequence (CPS) mode is a non-destructive contrast imaging technique that combines pulse inversion with amplitude modulation. After the b-mode scan, subsequent scans were taken in CPS mode (7 MHz, mechanical index = 0.18, CPS gain = -7 dB, dynamic range = 80 dB). The first CPS scan was taken as a baseline, before any contrast was injected to account for background noise and tissue harmonic signal. Consecutive scans were taken immediately after bolus injection of contrast for the first 3 minutes. Then, a scan was taken every 2 minutes until 10 minutes had passed to allow any unbound bubbles to clear. Lastly, a CPS scan was taken after the bubbles were destroyed using the 'D color' scan on the Sequoia. VEGF contrast was injected once in every animal (n=8), on every imaging day. An injection of control contrast was administered to at least one animal on every imaging day in order to look for differences in contrast targeting.

2.8 Image Analysis

MATLAB (Mathworks, Natick, MA) was used to convert each DICOM video file from the Sequoia into a stack of .tif images. MATLAB was used to draw regions of interest (ROIs) consisting of the tumor on the b-mode images, which were then applied to the contrast images **(Figure 2)**. In MATLAB, drawing an ROI creates a mask – all of the pixels inside the ROI are

set to 1, and all of the pixels outside the ROI are set to 0. The binary mask was then multiplied with the image, allowing us to analyze only the pixels within the ROI. A smoothing function was applied to the images to filter out the speckle (small dark regions). Then, a lower threshold was applied to detect the large dark regions within the image, and an upper threshold was applied to detect artifact. Pixels that fell outside of the designated range were eliminated via creation of another binary mask. The intensity of the pixels within each slice was averaged to give a resulting average intensity of the entire contrast scan.

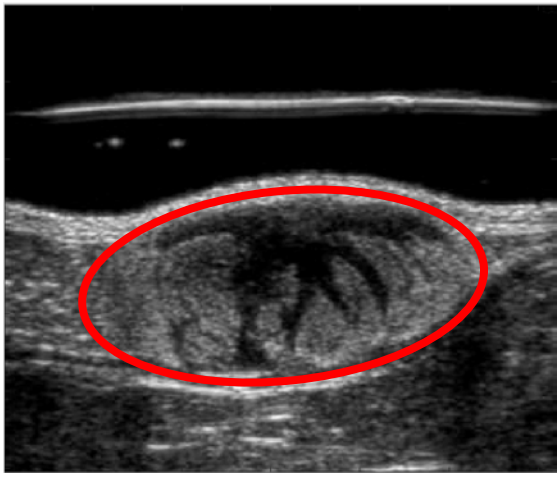

Figure 2*. Example region of interest (ROI). The b-mode scan was used to draw an ROI around the tumor (red line). This allows for analysis of only the pixels within the tumor ROI.*

The average intensity from each injection was plotted against time post injection to create time-intensity curves (TIC). Since each animal was imaged using VEGF contrast on every imaging day, a time-intensity curve was created after every contrast injection. **Figure 3** displays a sample time-intensity curve that compares the intensity between the ROI and tissue background up to 10 minutes post injection in an animal on day 1 post treatment. The tissue background values were determined by drawing an ROI outside of the tumor. Based on the perfusion rates of the contrast, the timepoint that was chosen to represent "targeted" or bound microbubbles was the scan taken at 2 minutes. At the 2-minute timepoint, signal from the

background tissue was minimal; however, there was still sufficient intensity within the ROI. To get the overall targeted intensity value, the average intensity from the scan taken post microbubble destruction was subtracted from the average intensity from the scan taken at 2 minutes.

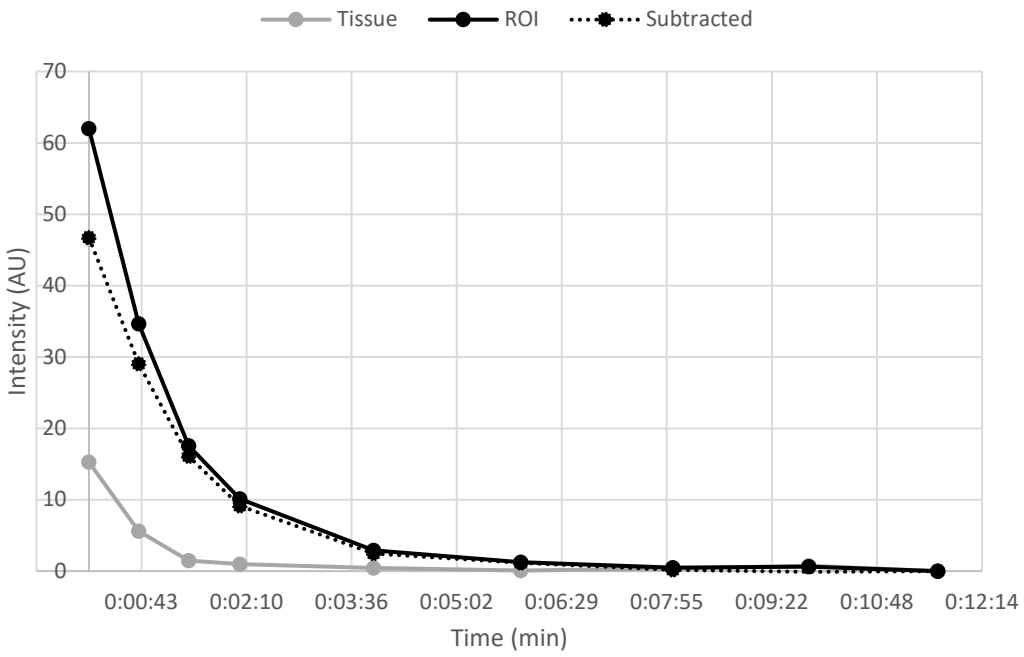

Figure 3. Example time-intensity curve (TIC) from day 1 post-treatment (n=1). *Comparison of the time-intensity between the region within the tumor ROI and tissue background. The dashed line represents the intensity within the tumor ROI after the tissue background signal is subtracted.*

Each targeted value was then divided by the peak signal intensity observed on the TIC.

$$\text{Molecular Targeting} = \frac{2\,min\ timepoint}{max\ intensity}$$

This was done to further account for necrosis and to try and account for changes in microbubble dose and size. These values were normalized by dividing by the initial baseline pre-treatment (day 0) value.

$$\text{Normalized Molecular Targeting on Day X} = \frac{Molecular\ Targeting\ on\ Day\ X}{Molecular\ Targeting\ on\ Day\ 0}$$

While it is known that the data outputted from the Sequoia is log compressed [11], for the purposes of this study, the intensity data was treated as linear, arbitrary values, and plotted as such. An attempt to linearize the log compressed data was made by taking each data point and plugging it into the formula, $y = 10^x$, where x is the data from the Sequoia and y is the linearized value. However, it became unfavorable to present the data as such due to the large range of raw targeted intensity and peak perfusion values. Using this technique, it was not possible to plot all the animal curves on one plot due to issues with scale. Tumor volume measurements were also taken throughout the study. They were also normalized to tumor volume on day 0 prior to treatment (baseline) and plotted.

$$\text{Normalized Tumor Volume on Day X} = \frac{Tumor\ Volume\ \ on\ Day\ X}{Tumor\ Volume\ on\ Day\ 0}$$

2.9 Statistical Methods

Statistical analysis was done to analyze the significance between molecular targeting on days 0 and 1, 1 and 3, and 14 and 17. A Kolmogorov-Smirnov normality test was used to determine that the distributions were indeed Gaussian, and thus paired t-tests were used to compare the calculated molecular targeting values between the same cohort of animals on different days.

3. Results

Unfortunately, the two untreated control animals died prior to the end of the study (day 3) and have therefore been excluded from the analysis.

3.1 Tumor Volume

Tumor volume was measured, and molecular imaging was performed on each animal until the tumor reached 2 cm in diameter. Tumor volume generally exhibits three phases after radiation treatment [5]. There is an initial negative treatment response phase where tumor

volume increases, followed by a response phase characterized by a decrease in tumor volume. Then, animals who do not respond to treatment exhibit a third phase that involves tumor regrowth [5]; in this study, these animals are classified as “non-responders”. The results indicate that all tumors (n=8) displayed an initial response phase post treatment (tumor size initially decreased). Out of the 8 treated animals, 6 were definite non-responders, meaning they experienced tumor regrowth. The other 2 animals expired before their tumors started to grow again, but for the purposes of the data analysis, all 8 animals were categorized as non-responders. For most of the animals, tumor volume began to regrow around day 17 post treatment. The average initial tumor volume was 905.7 mm^3 with a standard deviation of 343.9.

Tumor volume was normalized by dividing each tumor volume measurement by the baseline day 0 measurement. Thus, the tumor volume at day 0 was equal to 1 for every animal. The results were plotted (**Figure 4**).

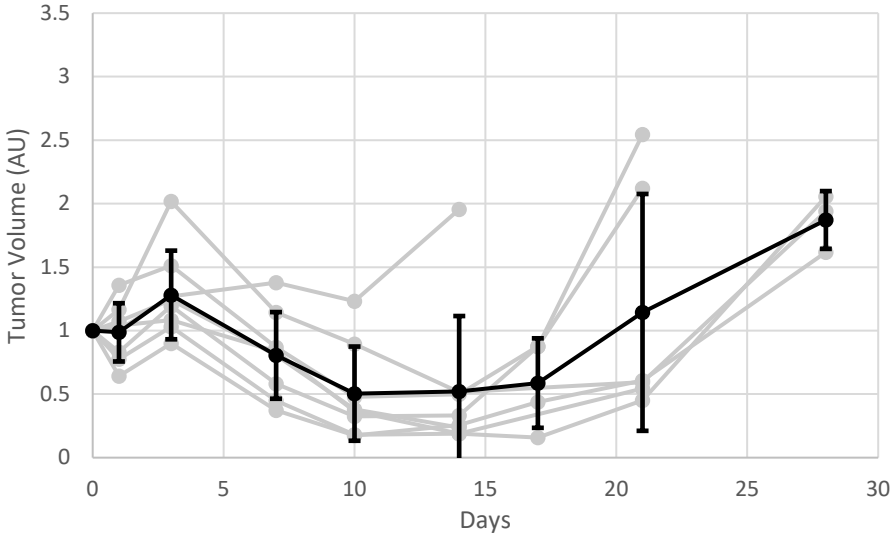

Figure 4. Tumor volume evolution over time post-treatment (n=8). *The black line represents the average of the entire group (error bars represent standard deviation). The lighter gray lines represent the data from each individual animal. Tumor volume was normalized by dividing by initial tumor volume prior to radiotherapy treatment.*

3.2 Molecular Targeting

As mentioned earlier, the average intensity value at 2 minutes was divided by the peak intensity value observed from the corresponding time-intensity curve from that injection to calculate molecular targeting. These molecular targeting values were normalized by dividing each molecular targeting value by the pre-treatment molecular targeting. The results were plotted (**Figure 5**). Overall, there is a decrease in molecular targeting between day 0 and day 28. Paired t-tests were used to determine the significance of the difference in molecular targeting between different days. There was a statistically significant decrease in molecular targeting between day 0 and day 1 (pre and post radiation therapy) ($p = 0.0002$). There was an increase in molecular targeting between days 1 and 3; however, this was not statistically significant ($p = 0.2736$). There was also an increase in molecular targeting between days 14 and 17, but this was also not significant ($p=0.5780$).

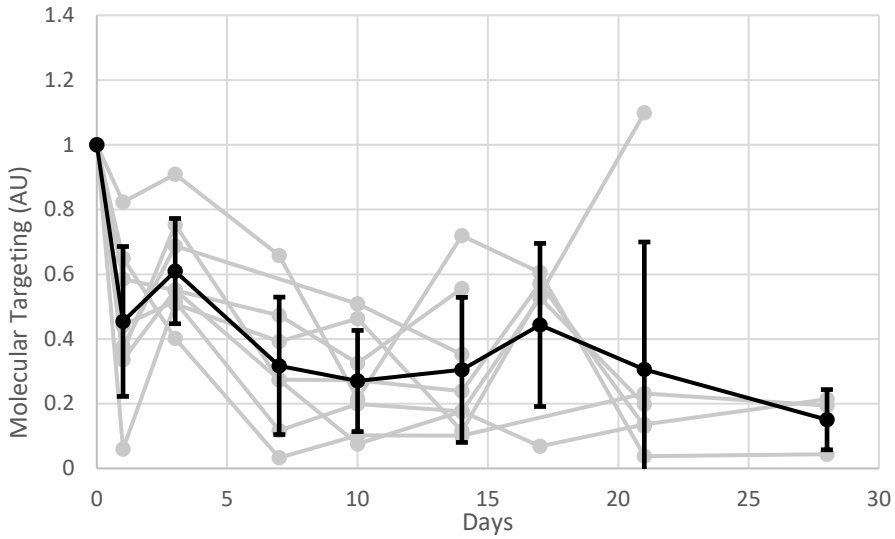

Figure 5. Calculated molecular targeting (MT) in the tumors over the course of the study (n=8)*. After each contrast injection, the intensity of the pixels within the tumor ROI was plotted with respect to time, creating a time-intensity curve (TIC). Molecular targeting was calculated by dividing the intensity within the tumor ROI at 2 minutes by the peak intensity on the TIC. The black line represents the average of the entire group (error bars represent standard deviation). The lighter gray lines represent the data from each individual animal. MT was normalized by dividing by baseline MT (prior to RT).*

As previously stated, the average intensity from each injection was plotted against time post injection to create time-intensity curves (TIC) for every animal, on every imaging day. The average area under the time-intensity curves was calculated, normalized by dividing by baseline AUC prior to RT, and then plotted (**Figure 6**). The area under the TIC decreased consistently throughout the study except for a slight increase around day 3. The maximum intensity value observed from the TIC was also normalized by dividing by baseline maximum intensity prior to RT and plotted (**Figure 7**). The maximum intensity also decreased overall between day 0 and day 28 of imaging.

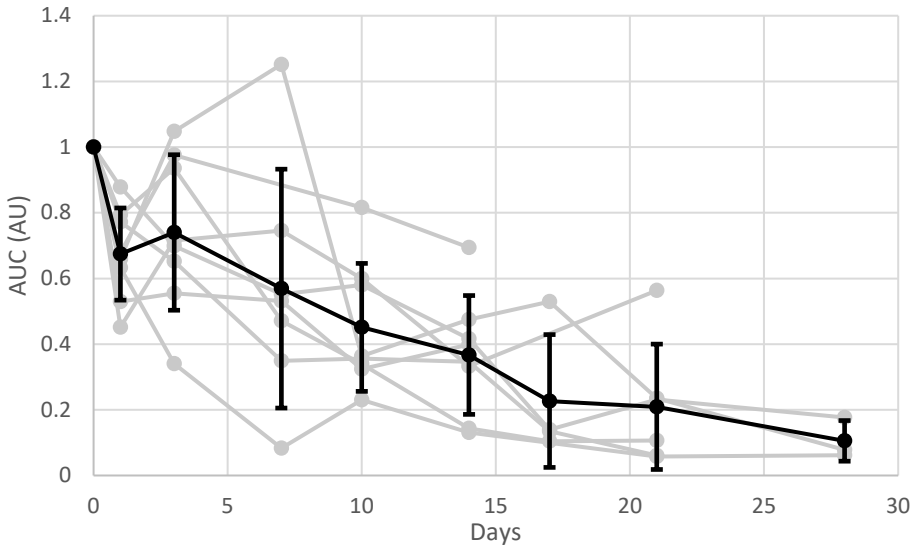

Figure 6. Calculated area under time-intensity curve (AUC) over the course of the study (n=8)*. After each contrast injection, the intensity of the pixels within the tumor ROI was plotted with respect to time, creating a time-intensity curve (TIC). The area under the TIC was calculated. The AUC values were normalized by dividing by the calculated baseline day 0 value (prior to RT). The black line represents the average of the entire group (error bars represent standard deviation). The lighter gray lines represent the data from each individual animal.*

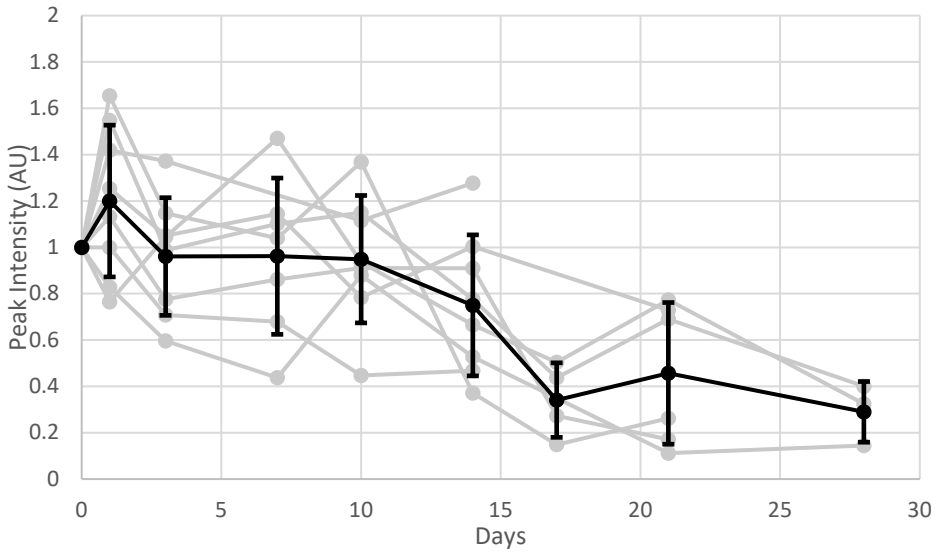

***Figure 7. Peak intensity observed from time-intensity curve over the course of the study (n=8)**. After each contrast injection, the intensity of the pixels within the tumor ROI was plotted with respect to time, creating a time-intensity curve (TIC). The peak intensity value observed on the TIC was normalized by dividing by the peak intensity value observed on baseline day 0 (prior to RT), and plotted. The black line represents the average of the entire group (error bars represent standard deviation). The lighter gray lines represent the data from each individual animal.*

Average molecular targeting was plotted against average tumor volume (**Figure 8**). The two curves exhibit similar behavior until after day 17. After day 17, molecular targeting decreases until day 28, while tumor volume increases.

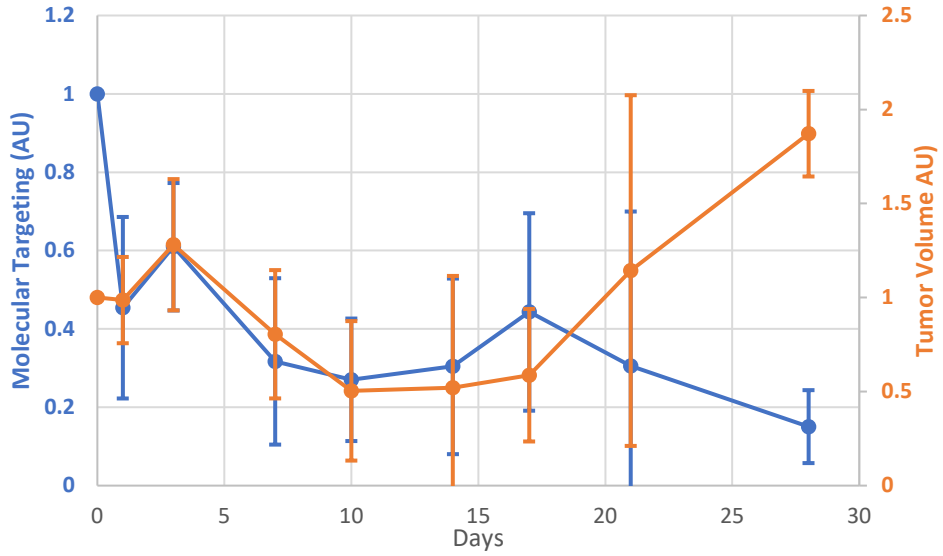

Figure 8. Average Molecular Targeting (MT) vs. Average Tumor Volume (TV) over the course of the study (n=8)*. Average MT is plotted on the left axis, while average TV is plotted on the right. Tumor volume was normalized by dividing by initial tumor volume on day 0 prior to radiation treatment (RT). After each contrast injection, the intensity of the pixels within the tumor ROI was plotted with respect to time, creating a time-intensity curve (TIC). Molecular targeting was calculated by dividing the intensity within the tumor ROI at 2 minutes by the peak intensity* on the TIC. *Molecular targeting was normalized by dividing by initial calculated molecular targeting on day 0 prior to RT. Error bars represent standard deviation.*

3.3 Control Contrast Data

Control contrast was also injected in at least one animal per imaging session. The time-intensity curves (TIC) for the control contrast were plotted and compared to the TIC for the targeted contrast that was injected in the same animal. In **Figure 9**, the time-intensity curve of the VEGF bubbles is compared to the time-intensity curve of the IgY bubbles in the same animal on day 7 post treatment. The calculated targeted molecular targeting of the VEGF bubbles was 0.17, while the calculated molecular targeting of the IgY bubbles was 0.38. The same comparison was made between the time-intensity curves of the VEGF bubbles and the NeutrAvidin control bubbles on day 17 post treatment (**Figure 10)**. The calculated molecular targeting from the VEGF bubbles was 0.24, while the targeted intensity value from the NeutrAvidin control bubbles was 0.17.

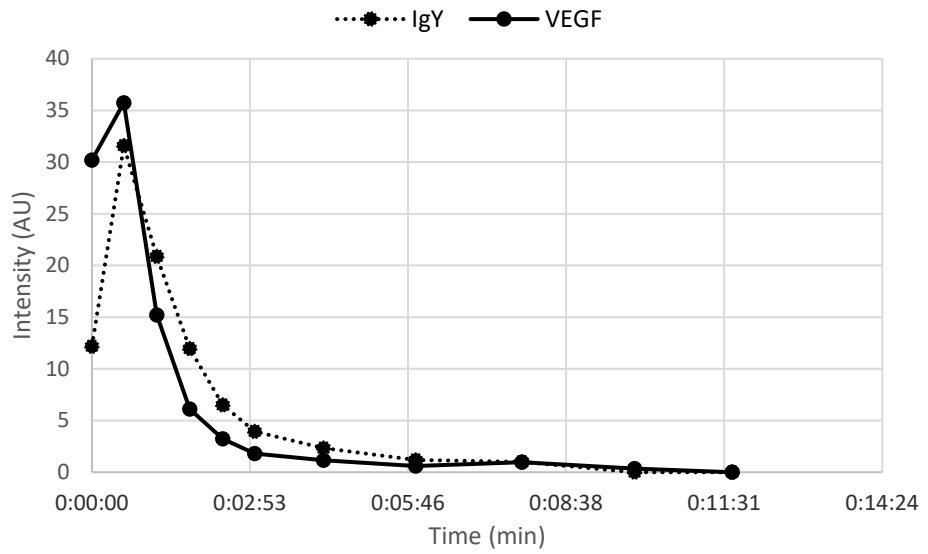

Figure 8. Intensity of VEGF contrast within tumor ROI compared to intensity of IgY contrast on day 7 post treatment (n=1). *After each contrast injection, the intensity of the pixels within the tumor ROI was plotted with respect to time, creating a time-intensity curve (TIC) as displayed in this figure. Molecular targeting was calculated by dividing the intensity within the tumor ROI at 2 minutes by the peak intensity on the TIC. Molecular targeting of VEGF contrast = 0.17. Molecular targeting of IgY contrast = 0.38.*

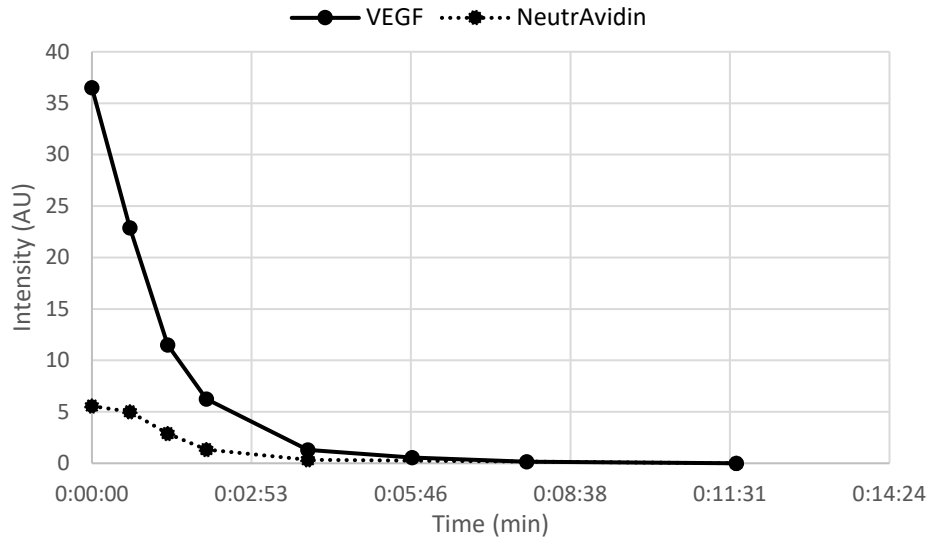

Figure 9. Intensity of VEGF contrast within tumor ROI compared to intensity of NeutrAvidin control contrast on day 17 post treatment (n=1). *After each contrast injection, the intensity of the pixels within the tumor ROI was plotted with respect to time, creating a time-intensity curve (TIC) as displayed in this figure. Molecular targeting was calculated by dividing the intensity within the tumor ROI at 2 minutes by the peak intensity on the TIC. Molecular targeting of VEGF contrast = 0.24. Molecular targeting of IgY contrast = 0.17.*

4. Discussion

This study aimed to use molecular imaging to assess tumor response to radiation therapy earlier than changes in tumor volume or vascular density. Molecular imaging was performed using microbubble contrast agents that targeted VEGFR-2. Animals were baseline imaged, treated with 20 Gy broad beam radiation, and then imaged twice a week thereafter. Results showed no significant increase in molecular targeting before increase in tumor volume. There were several issues with this study that need to be addressed.

4.1 Analysis Limitations

Firstly, the lack of untreated control data makes it difficult to draw any conclusions from the results. Moreover, even if the control animals had not died, a study with only 10 animals lacks statistical power and would need to be repeated several times to ensure reproducibility. Another limitation of the analysis that was mentioned earlier is the fact that the data from the Sequoia is log compressed. In this study, the average pixel intensities were treated as linear for ease of analysis; the occurrence of several other confounding variables made it clear that the study would need to be repeated in the future anyhow. However, future studies should linearize the log compressed data using the methods described in [15].

4.2 Variable Tumor Response

In the pilot study, there were 6 responders and 2 non-responders (**Supplemental Information S.2**). It is known that initial tumor size correlates negatively with response to radiation therapy [5]. For this study, the primary interest was in the non-responder category to determine whether the molecular targeting increased before the tumor regrowth phase. As a result, treatment was delayed until the tumors were approximately 1 cm in diameter to ensure that most of the cohort consisted of non-responders. The larger initial tumor size led to the

treatment of these tumors with 20 Gy rather than 15 Gy. However, the initial tumor size was likely too large; the entire treatment group was non-responders. Again, this limits any conclusions we can make from trends in the data due to the inability to compare results between responder and non-responder groups. **Table SI.1** displays the initial tumor volumes from both the pilot study and final study.

Another variable to consider is the tumor passage number. The initial fibrosarcoma tissue was provided by the Dewhirst Lab at Duke University (original stock). When tissue from the original stock is implanted into an animal, that is passage #1. Each time the tumor tissue is passed from one animal to the next is considered an additional passage. Tumors at higher passage numbers grow and behave irregularly; the passage number for the tumor tissue that was used in this study was on the higher end, which may be another factor that caused the entire cohort to be non-responders. It is difficult to control how many responders and non-responders are going to emerge within each cohort due to not only initial tumor size and dose variations but also the tumor passage number.

Prior to this molecular imaging study being repeated, a preliminary study should be done to see if it is possible to predict the number of responders and non-responders within several cohorts of rats. Three groups of rats could have different tumor passage numbers (low, medium, high), but similar initial tumor sizes. Three more groups could be from the same passage but treated when tumors are different sizes (small, medium, large). Lastly, each of these two groups could be further divided based on radiation treatment dose. This information would be valuable because it could allow for greater selection of and control over treatment response groups for future studies relating to assessment of response to radiation therapy.

4.3 Microbubble Inconsistencies

The average pixel intensity at maximum perfusion and at 2 minutes decreased for all the animals from day 0 to day 28. This was also observed in the pilot study **(Supplemental Information S.2**) and was thought to be due to the accelerated blood clearance effect. However, the phenomenon was observed again, even after pre-dosing to account for accelerated blood clearance. A reason for this could be that the animals were not pre-dosed with enough bubbles or for a long enough time. For next time, it is recommended that the animals are pre-dosed for at least 15 days prior to imaging.

The overall decrease in molecular targeting was likely caused by changes in the microbubble size distribution. It is known that the intensity observed on the Sequoia correlates strongly with microbubble size. For future long-term studies, any changes, (regardless of how slight) in the microbubble size distribution need to be considered. **Table SI.2** displays the microbubble size distribution at the beginning, middle, and end of the study.

Differences in microbubble size also caused issues with the comparison between the control contrast and the VEGF contrast. The bubbles in both types of control contrast were larger than the VEGF bubbles, which made the pixel intensity from the control contrast appear brighter. This may have caused the IgY bubbles to have a greater molecular targeting value than the VEGF bubbles.

Moreover, another limitation of this study is the fact that microbubble dose needs to be kept as uniform as possible between injections. Microbubble dose is difficult to control beyond measuring the concentration prior to imaging due to variances caused by pipette error and administration of the bubbles into the tail vein catheter. However, changes in microbubble size throughout a longitudinal study like this one can be accounted for by characterizing the

microbubble response using a tissue mimicking phantom before imaging every day and adjusting the data accordingly. Lastly, comparison of in house bubbles with a commercially available VEGFR-2 specific contrast agent should also be considered as a potential future study parameter.

4.4 Microbubble Circulation/Targeting Issues

In this study, it was presumed that all free-flowing bubbles had washed out by 2 minutes; this assumes uniform perfusion speed amongst animals. Perfusion speed can be affected by each animals' blood pressure, weight, age, etc. The rate of microbubble perfusion within an individual animal can also change over the course of the study, especially in response to radiation therapy. On a similar note, the short, 2 minute duration of targeting was alarming. Previous studies using VEGF targeted microbubbles in rats have used a targeted timepoint value of 7 min or greater [20].

The injected dose of 4×10^7 microbubbles was chosen based on experimental trial and error from the pilot study (**Supplemental Information S.1**). Perhaps the dose that was used for this study was not the optimal dose for this cohort of rats due to differences in size and age. The animals used in this study were older and had been imaged for a previous experiment some months prior (another confounding variable).

One reason why we think the dose was not optimal was because there was very little signal from the tissue background immediately after injection. This indicates that either there was not enough contrast being injected, or that perfusion happened quickly between scans. Another limitation of this study was the fact that a linear array transducer was used. The transducer had to step through the entire length of the tumor and then start from the beginning to start another scan. This resulting delay causes data loss, especially as the contrast is washing in.

In **Figure 3**, the tissue background was subtracted from the average pixel intensity within the tumor ROI. However, because of the aforementioned reasons, the tissue background was not subtracted from the ROI intensity for the molecular targeting analysis.

Microbubble dose needs to be optimized based on each animal cohort. This could be done by conducting a test imaging session prior to the start date of the study to experiment with the dose. Moreover, a lab database could be created to record the tumor/animal model, average animal age, average animal weight and sufficient microbubble dose so future imaging studies can be optimized more easily based on previous work. Furthermore, the delay and subsequent data loss caused by the linear array transducer could be eliminated by using a 2-D array that can simultaneously image the entire volume of the tumor. This would also allow for timepoints to be more consistent. The timepoints of the scans in the continuous 0-3-minute acquisition phase all varied slightly due to differences in the size of each tumor and the amount of time it took to step through the entire volume. Furthermore, a possible method to account for differences in perfusion speed between different animals would be to compare the targeted injections to control injections. The “targeted” timepoint could be selected based on when the control contrast seems to clear. This method was considered for this study; however, the new protocol would involve doing two contrast injections for every animal on a given imaging day and was not feasible due to time. Lastly, although tissue background was not subtracted from the ROI intensity for the analysis completed in this study, this should be done for future studies.

4.5 Complexities of VEGF Pathway

Another confounding variable in this study is the intricate nature of the VEGF pathway. One possible reason for the issues with molecular targeting could be the endocytosis of the VEGF-VEGFR-2 complex [21]. If there is an increase in VEGF-VEGFR-2 binding in the tumor,

but the complex is endocytosed into the cell, the microbubble would be unable to bind. This could explain why the increase in VEGF expression is not correlated with an increase in targeting signal. Moreover, the relationship between the number of VEGF receptors and secretion of VEGF is complex and not fully understood. If the number of receptors is staying the same, but the amount of free-flowing VEGF is increasing, then that poses a flaw with our experimental model; we assume that the number of VEGF receptors increases, which allows for increased microbubble binding. Another point to consider is the location of the increased VEGF expression. If VEGF is primarily being expressed on tumor vasculature, rather than the inner tumor cells, then it would make sense that most of the microbubble targeting occurs around the periphery of the tumor. This explains why the signal intensity on the inside of the tumors is so low and brings into question whether an ROI should be drawn around the entire tumor. In fact, the signal intensity was so low that removal of the necrotic areas of each tumor had little to no effect on the calculated molecular targeting values. Perhaps in the future, only the targeting observed around the tumor periphery may be used for the analysis. Other future directions of this study include the use of different molecular targets upstream or downstream of VEGF in the angiogenesis pathway. Furthermore, an anti-VEGF drug could be administered to a subset of the animals in order to compare the levels of molecular targeting between groups.

5. Conclusions

Molecular imaging is a promising application of contrast enhanced ultrasound that allows for characterization of biomarker expression in vivo. However, further optimization of molecular imaging parameters and data analysis is required to conduct a longitudinal study. Additionally, a further in-depth analysis regarding the complex molecular processes involved with VEGF/VEGFR regulation is required. The data from this study sheds light on the issues involved

with longitudinal molecular imaging, however the current methodological limitations do not allow for definitive conclusions regarding VEGFR-2 expression after radiotherapy in the rat FSA model. For this reason, the main takeaway of this work remains that the following studies should be undertaken prior to repeating this work: better prediction of tumor response (based on initial tumor size, tumor passage number, and radiation dose), characterization of microbubble response before imaging and subsequent adjustment of the data to account for differences in microbubble size, and completion of a molecular imaging study where the chosen "targeted" timepoint is variable and determined based on a control contrast injection.

6. Acknowledgements

The author would like to thank Dr. Sha Chang and the UNC Department of Radiation Oncology for providing access to the clinical linear accelerator that was used to treat the animals. The author would also like to acknowledge the following people from the UNC-NC State Joint Department of Biomedical Engineering: Sunny Kasoji for his mentorship, Thomas Kierski for his assistance with imaging the animals, Dr. James Tsuruta for microbubble contrast formulation, and lastly, Dr. Paul Dayton for providing the funding and resources necessary to conduct this experiment.

References

[1] Lu Y-F, Goldstein DB, Angrist M, Cavalleri G. Personalized Medicine and Human Genetic Diversity. Cold Spring Harbor Perspectives in Medicine. 2014;4(9):a008581. doi:10.1101/cshperspect.a008581.

[2] Mullane SA, Van Allen EM. Precision medicine for advanced prostate cancer. Current opinion in urology. 2016;26(3):231-239. doi:10.1097/MOU.0000000000000278.

[3] Radiation Therapy for Cancer. National Cancer Institute. https://www.cancer.gov/about-cancer/treatment/types/radiation-therapy/radiation-fact-sheet#q1. 2017.

[4] Eisenhauer EA, Therasse P, Bogaerts J, Schwartz LH, Sargent D, Ford R, et al. New response evaluation criteria in solid tumours: Revised RECIST guideline (version 1.1). Eur. J. Cancer. 2009; 45(2):228–247. doi:10.1016/j.ejca.2008.10.026.

[5] Kasoji SK, Rivera JN, Gessner RC, Chang SX, Dayton PA. Early assessment of tumor response to radiation therapy using high-resolution quantitative microvascular ultrasound imaging. Theranostics. 2018; 8(1):156-168. doi:10.7150/thno.19703.

[6] Burney IA, Lakhtakia R. Precision Medicine: Where have we reached and where are we headed? Sultan Qaboos University Medical Journal. 2017;17(3):e255-e258. doi:10.18295/squmj.2017.17.03.001.

[7] Maeda A, Leung MKK, Conroy L, et al. *In Vivo* Optical Imaging of Tumor and Microvascular Response to Ionizing Radiation. Bogyo M, ed. PLoS ONE. 2012;7(8):e42133. doi:10.1371/journal.pone.0042133.

[8] Anderson CR, Rychak JJ, Backer M, Backer J, Klibanov AL. scVEGF microbubble ultrasound contrast agents: a novel probe for ultrasound molecular imaging of tumor angiogenesis. Investigative radiology. 2010;45(10):579-585. doi:10.1097/RLI.0b013e3181efd581.

[9] Greijer AE, van der Wall E. The role of hypoxia inducible factor 1 (HIF-1) in hypoxia induced apoptosis. Journal of Clinical Pathology. 2004;57(10):1009-1014. doi:10.1136/jcp.2003.015032.

[10] Duffy AM, Bouchier-Hayes DJ, Harmey JH. Vascular Endothelial Growth Factor (VEGF) and Its Role in Non-Endothelial Cells: Autocrine Signalling by VEGF. In:

Madame Curie Bioscience Database [Internet]. Austin (TX): Landes Bioscience; 2000-2013. Available from: https://www.ncbi.nlm.nih.gov/books/NBK6482/

[11] Bergers G, Song S. The role of pericytes in blood-vessel formation and maintenance. Neuro-Oncology. 2005;7(4):452-464. doi:10.1215/S1152851705000232.

[12] Abou-Elkacem L, Bachawal SV, Willmann JK. Ultrasound molecular imaging: moving towards clinical translation. European journal of radiology. 2015;84(9):1685-1693. doi:10.1016/j.ejrad.2015.03.016.

[13] Tan S, Teh H, Mancer JK, Poh W. Improving B mode ultrasound evaluation of breast lesions with real-time ultrasound elastography—A clinical approach. The Breast. 2008;17(3):252-257. doi:10.1016/j.breast.2007.10.015.

[14] Borden MA, Streeter JE, Sirsi SR, Dayton PA. In vivo demonstration of cancer molecular imaging with ultrasound radiation force and buried-ligand microbubbles. Mol Imaging. 2013; 12(6):357-262.

[15] Tsuruta JK, Schaub NP, Rojas JD, Streeter J, Klauber-DeMore N, Dayton P. Optimizing ultrasound molecular imaging of secreted frizzled related protein 2 expression in angiosarcoma. Arbiser J, ed. PLoS ONE. 2017;12(3):e0174281. doi:10.1371/journal.pone.0174281.

[16] Streeter JE, Gessner R, Miles I, Dayton PA. Improving Sensitivity in Ultrasound Molecular Imaging by Tailoring Contrast Agent Size Distribution: In Vivo Studies. Molecular imaging. 2010;9(2):87-95.

[17] Holmes K, Roberts OL, Thomas AM, Cross MJ. Vascular endothelial growth factor receptor-2: structure, function, intracellular signalling and therapeutic inhibition. Cell Signal. 2007 Oct;19(10):2003-12. Epub 2007 Jun 12.

[18] Karkkainen MJ, Petrova TV. Vascular endothelial growth factor receptors in the regulation of angiogenesis and lymphangiogenesis. Oncogene. 2000 Nov 20;19(49):5598-605.

[19] Fix SM, Nyankima AG, McSweeney MD, Tsuruta JK, Lai SK, Dayton PA. Accelerated clearance of microbubbles containing polyethylene glycol (PEG) is associated with the generation of anti-PEG antibodies. Ultrasound Med Biol. 2018 Mar 27. pii: S0301-5629(18)30072-3. doi: 10.1016/j.ultrasmedbio.2018.02.006.

[20] Rojas JD, Lin F, Chiang Y-C, et al. Ultrasound Molecular Imaging of VEGFR-2 in Clear-Cell Renal Cell Carcinoma Tracks Disease Response to Antiangiogenic and Notch-Inhibition Therapy. Theranostics. 2018;8(1):141-155. doi:10.7150/thno.19658.

[21] E G, Cao Y, Bhattacharya S, Dutta S, Wang E, Mukhopadhyay D. Endogenous Vascular Endothelial Growth Factor-A (VEGF-A) Maintains Endothelial Cell Homeostasis by Regulating VEGF Receptor-2 Transcription. The Journal of Biological Chemistry. 2012;287(5):3029-3041. doi:10.1074/jbc.M111.293985.

Supplemental Information – Pilot Study

This study was completed from August to December 2017 as part of BME course 691H by Ruby Patel. It formed the basis of the current work presented in this thesis and is therefore included as relevant background for the methods chosen in the current study.

S.1 Materials and Methods

Rat fibrosarcoma tumor tissue was subcutaneously implanted into the right flank for female Fischer 344 rats (n=10) (Charles River Laboratories, Durham, NC). Once tumors grew to 5-10 mm, 8 animals were given a single dose of 15 Gy broad beam radiation and 2 were left as untreated controls.

The injected volume of microbubbles was adjusted based on the daily concentration such that each injection contained approximately 4×10^7 microbubbles. This value was chosen based on experimental trial and error such that sufficient targeting was present. The same transducer and ultrasound system as the one described in the final study were used for imaging. The animals were imaged one day prior to radiation treatment (baseline), one day after treatment and then every 2-3 days until the tumors were no longer visible or reached 2 cm in diameter.

The same protocol as the one mentioned in the final study was used to prepare the animal for imaging. A preliminary b-mode scan was taken before any contrast was injected. After the b-mode image, four scans were taken in CPS mode. The first CPS scan was taken as a baseline. The second image was taken immediately after bolus injection of contrast and depicted full perfusion. 3-7 minutes was allowed to pass to let any unbound bubbles clear and, after which a third CPS scan of the "bound" bubbles was taken. Lastly, the bubbles were destroyed, and CPS scan was taken afterwards.

MATLAB (Mathworks, Natick, MA) was used to convert each DICOM video file from the Sequoia into a .mat file. ROI's were drawn on the b-mode scan and applied to the contrast scans. The fully perfused image was used to create a mask that represented necrotic regions. A smoothing function was applied to the perfused image to filter out the speckle. Then, a threshold was applied to detect the large dark regions within the image, creating a mask. The necrosis mask was multiplied with the contrast images to account for tumor necrosis. The intensity of the pixels in the ROI within each slice was averaged to give a resulting average intensity of the entire contrast scan. To get the overall intensity value for each timepoint, the average post-destruction intensity was subtracted from the average targeted scan intensity.

The molecular targeting was calculated and normalized as described in the final study. Tumor volume measurements were also taken and normalized as described in the final study.

S.2 Results

Out of the 8 treated animals, 6 responded to treatment, and 2 did not respond to treatment. These classifications were made based on whether the tumor disappeared (responder) or continued to grow to 2 cm, the maximum allowable tumor size (non-responder). The average initial tumor volume was 262.6 mm^3 (standard deviation = 113.7) for the responders (n = 6), 313.2 mm^3 (standard deviation = 148.3) for the non-responders (n = 2), and 114.5 mm^3 (standard deviation = 18.6) for the controls. There was no significant difference between the initial tumor size of the responders and the non-responders (p = 0.62).

Overall, the tumor volume growth for each group exhibited expected behaviors. The tumor volume measurements from each day were averaged within each group and then plotted against imaging day (**Figure SI 1**).

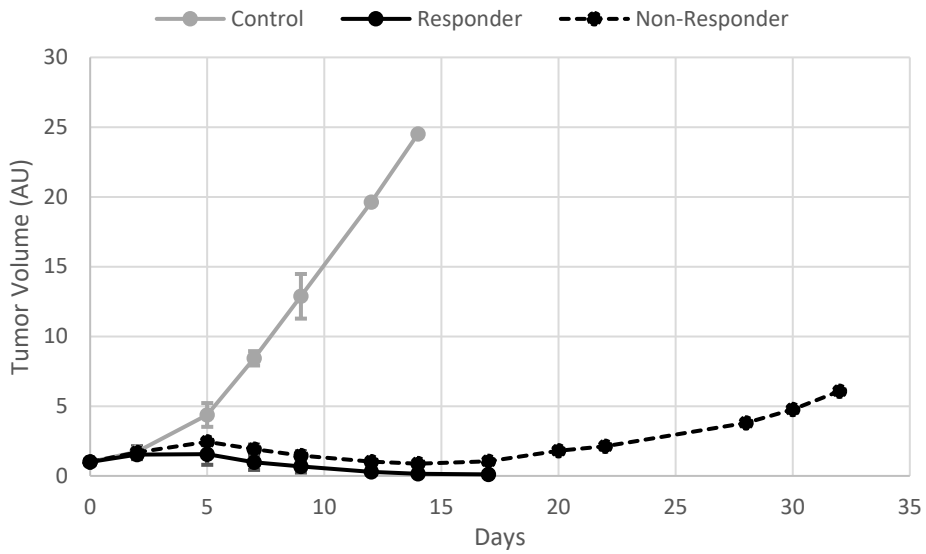

Figure SI 1. Tumor volume evolution within each response group – control (n=2), responder (n=6), and non-responder (n=2). *Tumor volume measurements were averaged within each*

group (error bars represent standard deviation) and plotted. Tumor volume measurements were normalized to baseline measurements taken prior to radiation treatment (day 0).

Molecular targeting values from each imaging day were averaged within each group and then plotted against imaging day (**Figure SI 2**). Overall, the control group had the highest levels of molecular targeting, followed by the responders, and then the non-responders. The responder and non-responder curves behaved somewhat similarly – an initial decrease in molecular targeting until day 7, followed by an increase until day 14.

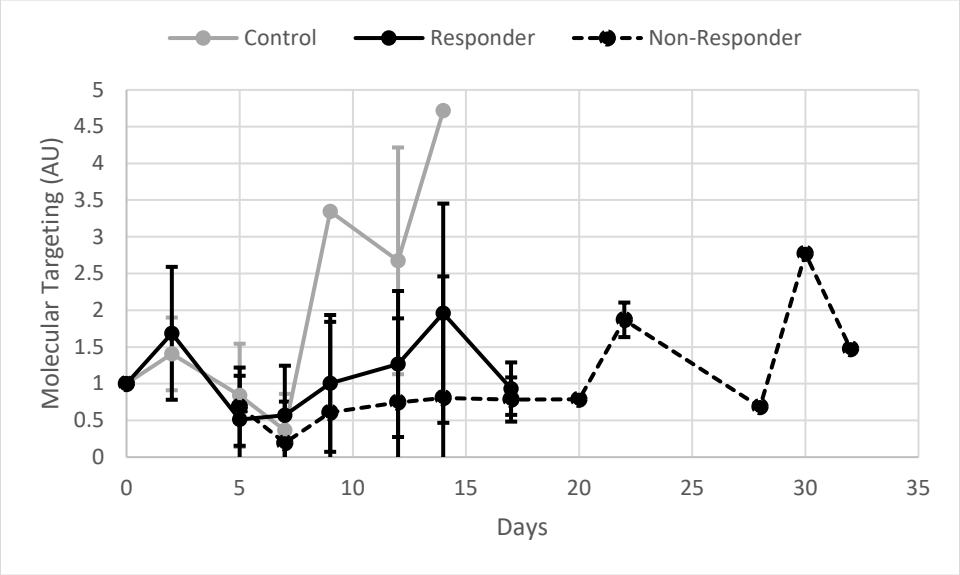

Figure SI 2. Molecular targeting (MT) evolution within each response group – control (n=2), responder (n=6), and non-responder (n=2). *After each contrast injection, the intensity of the pixels within the tumor ROI was plotted with respect to time, creating a time-intensity curve (TIC). Molecular targeting was calculated by dividing the intensity within the tumor ROI at 2 minutes by the peak intensity on the TIC. Calculated MT was averaged within each group (error bars represent standard deviation) and plotted. Calculated MT values were normalized to baseline measurements taken prior to radiation treatment (day 0).*

Average tumor volume and molecular targeting were also plotted on the same graph for each group. The responders' graph (**Figure SI 3**) shows that at day 5, tumor volume decreases and continues as such for the remainder of the study, while molecular targeting begins to increase. On the non-responders' graph (**Figure SI 4**), molecular targeting increased overall between days 7 and 32, but there were periods of targeting decrease during this interval. Tumor

volume increased, decreased, and then increased again. From Figures **SI 3** and **SI 4,** it is apparent that the responders have a more consistent level of molecular targeting, whereas the non-responders seem to exhibit larger differences in targeting between days. On the controls' graph (Figure **SI 5**), tumor volume steadily increased, while molecular targeting increased, then decreased, and then increased again.

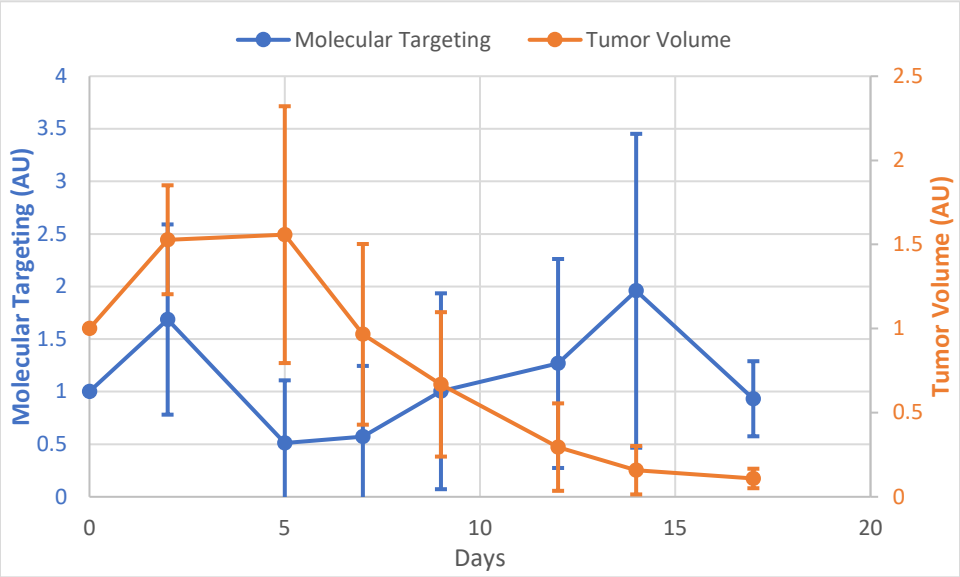

Figure SI 3. Average Molecular Targeting (MT) vs. Average Tumor Volume (TV) over the course of the study within the Responders group (n=6)*. Average MT is plotted on the left axis, while average TV is plotted on the right. Tumor volume was normalized to initial tumor volume on day 0 prior to radiation treatment (RT). After each contrast injection, the intensity of the pixels within the tumor ROI was plotted with respect to time, creating a time-intensity curve (TIC). Molecular targeting was calculated by dividing the intensity within the tumor ROI at 2 minutes by the peak intensity on the TIC. Molecular targeting was normalized to initial calculated molecular targeting on day 0 prior to RT. Error bars represent standard deviation.*

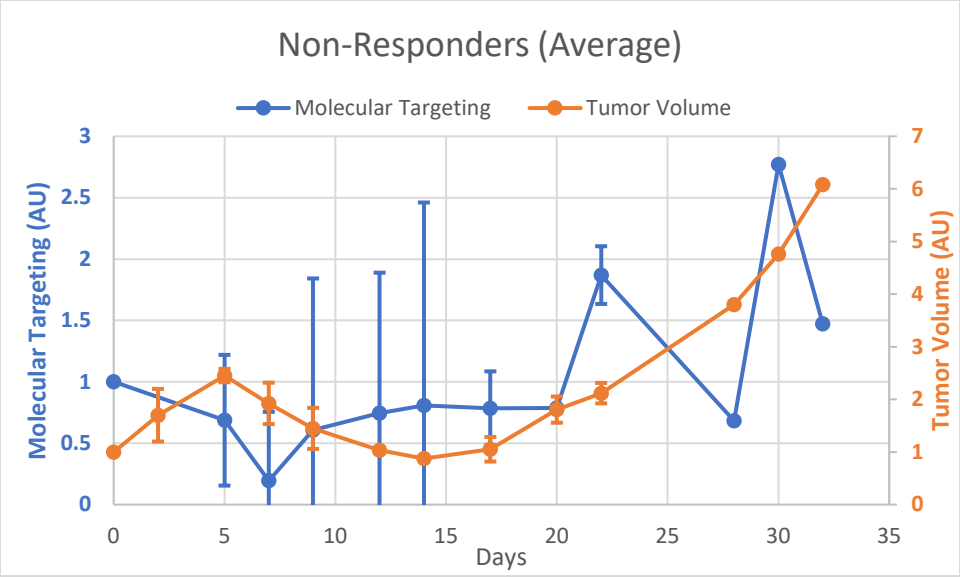

Figure SI 4. Average Molecular Targeting (MT) vs. Average Tumor Volume (TV) over the course of the study within the Non-Responders group (n=2). *Average MT is plotted on the left axis, while average TV is plotted on the right. Tumor volume was normalized to initial tumor volume on day 0 prior to radiation treatment (RT). After each contrast injection, the intensity of the pixels within the tumor ROI was plotted with respect to time, creating a time-intensity curve (TIC). Molecular targeting was calculated by dividing the intensity within the tumor ROI at 2 minutes by the peak intensity on the TIC. Molecular targeting was normalized to initial calculated molecular targeting on day 0 prior to RT. Error bars represent standard deviation.*

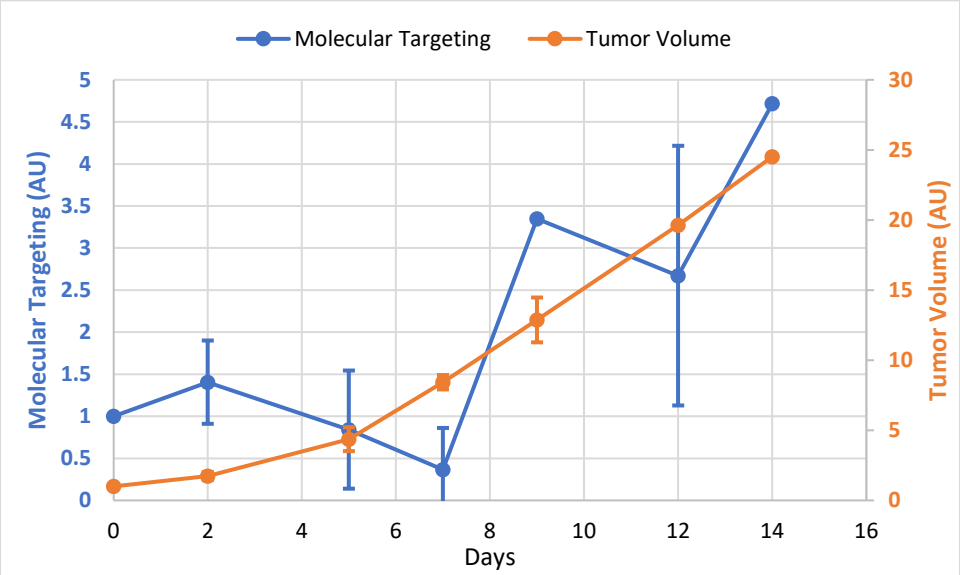

Figure SI 5. Average Molecular Targeting (MT) vs. Average Tumor Volume (TV) over the course of the study within the Control group (n=2). *Average MT is plotted on the left axis, while average TV is plotted on the right. Tumor volume was normalized to initial tumor volume on day*

0 prior to radiation treatment (RT). After each contrast injection, the intensity of the pixels within the tumor ROI was plotted with respect to time, creating a time-intensity curve (TIC). Molecular targeting was calculated by dividing the intensity within the tumor ROI at 2 minutes by the peak intensity on the TIC. Molecular targeting was normalized to initial calculated molecular targeting on day 0 prior to RT. Error bars represent standard deviation.

S.3 Discussion

There were several unexpected results from this pilot study. The overall molecular targeting signal was lower in the non-responder group than the responder group. Based on what we know about increased angiogenesis in tumors that are remodeling, we expect the opposite to be true. Moreover, it was also unclear why molecular targeting began to decrease as tumor volume increased in the initial response phase post-treatment. The data from the control animals was also peculiar because there was a decrease in targeting signal even as tumor volume began to increase. As tumor volume increases, we expected molecular targeting to also increase.

One confounding variable was the accelerated blood clearance (ABC) effect. The ABC effect is the immune response triggered by PEG, which is found on the microbubble shell. We initially had to wait 7-10 minutes for the unbound contrast to clear. After 2-3 days of imaging, the contrast was clearing faster and we only had to wait 3 minutes. It is important to note that the batch of microbubbles was changed after day 2. This could have accelerated the emergence of the ABC effect. Moreover, the microbubble dose was experimented with in the beginning, especially on imaging day 5, where the animals received 1×10^7 microbubbles instead of 4×10^7 microbubbles. Another variable that could have affected the results is the accuracy of the Accusizer. If the reported concentration of the contrast was slightly higher or lower than the actual value, the resulting dose of microbubbles injected into the animal would be slightly offset.

Additionally, the data from the non-responders group had only two animals. After day 22, the data reflects the results from just the final rat. This study needs to be repeated with more animals in every group, but especially the non-responder group.

S.4 Additional Supplemental Data

Group	Average Initial Tumor Volume (mm^3)	Standard Deviation
Pilot Study – Responder (n=6)	262.6	113.7
Pilot Study – Non-Responder (n=2)	313.2	148.3
Pilot Study – Control (n=2)	114.5	18.6
Final Study (n=8)	905.7	343.9

Table SI 1. Initial Tumor Volumes for the different studies, subdivided by responder/non-responder classification a posteriori.

Date	Mean (µm)	Standard Deviation	Median (µm)	Mode (µm)	Concentration (#/mL)
02-13-18	1.99	1.05	1.70	1.70	3e9
03-01-18	1.67	0.86	1.56	1.70	3e9
03-17-18	1.49	0.77	1.42	1.70	3e9

Table SI 2. VEGF Microbubble Size Distribution. *Microbubbles were sized every day prior to imaging using the AccuSizer. Values recorded here are diameters.*